Enhanced dielectric and electrical properties in CaZrO$_3$-doped X8R BaTiO$_3$-based ceramics sintered at medium temperature

Lingxia Li · Yaran Liu · Mingjing Wang ·
Ning Zhang · Junxiao Chen

Abstract Lead-free X8R BaTiO$_3$-based ceramics were prepared by conventional solid-state method. The influence of the composition and procedures on the microstructures, lattice parameters and dielectric properties of ceramics materials were systemically studied. XRD results indicate that no secondary phase is formed in the CaZrO$_3$-doped samples after sintering. The content of Ca^{2+} ions and Zr^{4+} ions decrease from grain boundaries to grain interiors referring to EDS results, which indicate that the ions mainly locate in the grain boundaries. The Curie temperatures of all CaZrO$_3$ doped samples increase due to the increasing tetragonality caused by the addition of CaZrO$_3$. SEM micrographs reveal that the grain size of CaZrO$_3$-doped BaTiO$_3$-based samples are not uniform, ranging from 0.2 to 0.8 μm. Furthermore, samples doped with 1.0 wt % CaZrO$_3$ exhibit optimal dielectric properties with high temperature stability of capacitance, due to the fine-grain microstructures. Moreover, we obtained a lead-free high performance X8R dielectric ceramic composition sintered at medium temperature (1,135 °C).

1 Introduction

There is a quickly growing requirement for multilayer ceramic capacitors (MLCC) with small size and large capacitance. X7R MLCC have been widely used for miniaturization of electronic components owing to their high dielectric constant and temperature-stable dielectric characteristics (from −55 to 125 °C, ΔC/C = ± 15 % of the capacitance at 25 °C or below) [1]. Since these electronic apparatuses are for stable engine controlling unit, drive controlling, programmed fuel injection and brake controlling, preferable temperature stability of the circuit is required. As these electronic components are subjected to the engine space under harsh temperature, capacitors are also required to have preferable temperature characteristics and, particularly, required to have a flat temperature characteristic under a higher operating temperature. Therefore, much attention has been paid to MLCC that satisfy the X8R characteristics of the Electronic Industries Alliance (EIA) standard (−55 to 150 °C, ΔC/C = ± 15 % of the capacitance at 25 °C or below) [2–4].

As a ferroelectric perovskite ceramic, barium titanate (BaTiO$_3$) exhibits a high permittivity at room temperature, making it suitable for applications in MLCC [5]. However, the permittivity of pure BaTiO$_3$ declines remarkably above the Curie temperature (125 °C), obeying Curie–Weiss law. Previous studies have demonstrated that to own a stable temperature coefficient of capacitance (TCC), an effect method is to shift T$_c$ to a high temperature [6]. It is reported that T$_c$ is increased effectively by introducing rare earth oxides, doping high T$_c$ value substances and ion substitution. (a) Introducing rare earth oxides: the increase in T$_c$ is attributed to the changes in internal stress caused by the substitution of rare earth elements in the shell region of a BaTiO$_3$ (BT) surface, referred to as a "core–shell" structure [7]. (b) High T$_c$ value substances doping: BaTiO$_3$ can also be modified by many dopants with high T$_c$ value e.g., Pb$_3$O$_4$, Bi$_2$O$_3$, Pb(Ti, Sn)O$_3$, PbTiO$_3$, PZT et al., to obtain a high dielectric constant and a broadened TCC curve [5, 8]. (c) Ion substitution:The substitution of Ba^{2+} with small ions or the substitution of Ti^{4+} with large ions makes the unit cells contact. The tensile stress stabilizes the tetragonal phase and shifts T$_c$ to a higher point [6, 9–11].

L. Li (✉) · Y. Liu · M. Wang · N. Zhang · J. Chen
School of Electronic and Information Engineering,
Tianjin University, Tianjin 300072, China
e-mail: llx66tju@163.com

Table 1 Lattice parameters of and electrical properties of CaZrO$_3$-doped BaTiO$_3$ samples in room temperature

Sample	CaZrO$_3$ content (wt %)	c (Å)	c/a	T$_c$ (°C)	Eb (kV/mm)	ρ$_v$ (10^{13} Ω cm)	ε$_r$	tgδ (%)	ΔC/C$_{20°C}$ (%)		
									−55 °C	125 °C	150 °C
CZ00	0.0	4.0083	1.0047	122.7	9.22	2.01	3,369	1.043	−12.8	12.1	−11.9
CZ05	0.5	4.0056	1.0042	123.9	10.35	2.15	3,325	1.025	−11.1	8.9	−11.4
CZ10	1.0	4.0052	1.0052	127.3	13.37	2.73	3,203	1.019	−10.0	5.8	−9.8
CZ20	2.0	4.0012	1.0022	124.9	10.43	2.63	3,279	0.958	−9.1	2.0	−13.9
CZ30	3.0	4.0122	1.0035	124.8	10.46	2.03	3,290	0.918	−8.0	3.2	−15.8

Many researchers have done a lot of work on ions doping in BaTiO$_3$ to improve dielectric properties, but most of their compositions sintered at elevated temperature which don't meet the need of medium sintering temperature (1,000–1,150 °C) when produce MLCC or their compositions included Pb which is not environmental [6, 12–14]. It is noteworthy that Ag70/Pd30 is a common electrode of MLCC, and it requires the sintering temperature of dielectric materials lower than 1,150 °C [8]. To meet the use of Ag70/Pd30 electrode, it's necessary to reduce the sintering temperature. Furthermore, in order to meet the request of environment-friendly materials, we chose CaZrO$_3$ as the dopants to obtain a flat TCC curve, which shifts T$_c$ value to a higher temperature [6]. In this paper, we investigated the effects of CaZrO$_3$ (0–3.0 wt %) on the dielectric and electrical properties of BT-based ceramics, and discussed the possible mechanisms. Most important, we prepared lead-free BT-based materials that satisfies the X8R characteristics, and the materials was sintered at medium temperature (1,135 °C). There is no use of rare earth elements in the materials system, and the experimental method is traditional solid state method, which is easy to achieve.

2 Experimental

2.1 Sample preparation

Samples with various amounts of CaZrO$_3$ were prepared by conventional solid-state method. The base material was BaTiO$_3$ powder (particle diameter about 500 nm, Guoci Co. Ltd., China). The additives included 0.2 wt % Niobium and manganese compounds (synthesized from MnCO$_3$ and Nb$_2$O$_5$ with the mole ratio of 2:1), 0.9 wt % Niobium and nickel compounds (synthesized from NiO and Nb$_2$O$_5$ with the mole ratio of 3:4), 5.0 wt % Glass flux (synthesized by 23.55 wt % Bi$_2$O$_3$, 19.85 wt % TiO$_2$, 24.30 wt % ZnO, and 32.30 wt % H$_3$BO$_3$) and various amounts of CaZrO$_3$ (0.0, 0.5, 1.0, 2.0 and 3.0 wt %). Ca-ZrO$_3$ was obtained after calcining the mixture of CaCO$_3$

and ZrO$_2$ at 1,000 °C for 2 h. Samples with various content of CaZrO$_3$ were prepared, as listed in Table 1. BT and all the additives were weighed and mixed with deionized water by ball milling (using ZrO$_2$ beads) for 4 h and then dried. After drying, mixed powders were added in 7 wt % binder wax, and then pressed into discs with 15 mm in diameter and 1 mm in thickness. The discs were sintered at 1,140, 1,135 and 1,130 °C for 3 h in air, using a heating rate of 5 °C/min. Silver was applied on both sides of the as-fired samples to obtain the electrodes of capacitors.

2.2 Characterization

Phase identification and lattice parameters were characterized by X-ray diffraction (XRD) patterns, which were obtained from D/MAX-B Model X-ray diffractometer (D8-Focus; Bruker AXS GmbH, Karlsruhe, German) with CuKa radiation at 40 kV and 40 mA. Microstructural properties such as grain size distribution and morphology were examined using a field-emission scanning electron microscopy (FE-SEM, S-4800; Hitachi, Ltd., Tokyo, Japan). Element distribution of separate areas was studied by energy-dispersive spectrometry (EDS). Dielectric loss and capacitance were measured by the use of capacitance meter (HP4278A; Hewlett-Packard, Santa Clara, CA) at 1 kHz from −55 to 150 °C. The temperature was controlled by GZ-ESPEC oven. Insulation resistivity was measured using a high resistance meter (Agilent 4339B, Santa Clara, CA) at room temperature. The frequency characteristics were measured between 50 Hz and 100 kHz, using a TH2828S automatic component analyzer.

3 Results and discussion

3.1 Solubility analysis

Figure 1 shows the XRD patterns of various amounts of CaZrO$_3$-doped BT-based ceramics sintering at 1,135 °C for 3 h. The XRD results demonstrate that all the samples display a desired perovskite structure, which indicates that
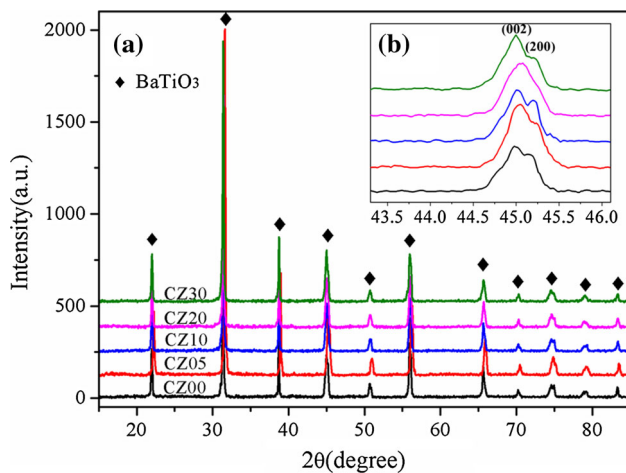
Fig. 1 XRD patterns of BaTiO$_3$ ceramic samples doped with various amounts of CaZrO$_3$ sintered at 1,135 °C

the CaZrO$_3$ have diffused into the BT lattice to form a solid solution [6, 13]. With the increasing CaZrO$_3$ content, the (200) and (002) peaks emerge into one peak and then split off slightly as shown in Fig. 1b. As we know, the tetragonal structure is characterized by (200) and (002) peak splitting around 45°, and the pseudo-cubic structure is characterized by (200) peak around 45° [3, 9, 15, 16]. Therefore, according to these characteristic peaks, it clearly indicates that the crystal structure changes gradually from tetragonal to pseudo-cubic with increasing CaZrO$_3$ content and that the phase converses from tetragonal to cubic. After that, the phase changes to tetragonal again.

Moreover, the variation of tetragonality can also be certified by the variety of c/a, which is attributed to the substitution of Ca^{2+} in the Ti-site. Armstrong et al. [17] figured that the great internal stress caused by the high expansion shell forced a decrease in the c lattice parameter and thus tetragonality decreased. The substitution of Ba^{2+} (1.61 Å, 12 coordinate) with Ca^{2+} (1.34 Å, 12 coordinate) makes the unit cells compact, while, when Ca^{2+} substitute Ti^{4+} (0.605 Å, six coordinate), the unit cells are expanded. The lattice parameters and the value of c/a with various CaZrO$_3$ amounts are presented in Table 1. When doped with small amount of CaZrO$_3$, Ca^{2+} mainly enter the A-sites which increase tetragonality, and then Ca^{2+} enter the B-sites with the continued increasing of CaZrO$_3$ content [18]. Accordingly, the lattice parameters reduce initially and then increase, therefore, the (200) and (002) peaks emerge into one peak and then split off slightly. The 1.0 wt % CaZrO$_3$-doped samples that exhibited the optimal tetragonal structure showed the superior dielectric properties, due to the reinforcement of Ti^{4+} ions' spontaneous polarization [4, 9].

3.2 Microstructure analysis

Microstructure and elements distributions have been studied by SEM and EDS. As can be seen in Fig. 2a–e, the grain size of CaZrO$_3$-doped BT-based samples are not uniform, ranging from 0.2 to 0.8 μm. The grain size increases gradually with increasing CaZrO$_3$ content, then some large grain produces due to the secondary grain growth, and no second phase is observed in all patterns. The microstructure of CZ00 sample is not compact for there are same pores. With the increasing CaZrO$_3$ content, the ceramics microstructure become more compact and uniform, and the pores decrease slightly. Among the samples, CZ10 is predominantly composed of fine grains (<1 μm) with smooth surface and clear boundaries. However, with the continued increasing of CaZrO$_3$ content, grain boundaries liquefies. This can be interpreted by the substitution of Ti^{4+} with Ca^{2+}, for the excess Ti^{4+} at grain boundary is known to easily form a eutectic liquid phase [10, 19], and this consequence is consistent with the XRD results. As we all know, the A/B ratio has a dramatic influence on sintering behavior. The excess Ti will react with BT to form eutectics, so liquid phase is available. The substitution of Ti with Ca^{2+} will bring about excess Ti and even lower the eutectic temperature. Thus, it make it's possible to sinter at medium temperature. To conclude, many benefits can be expected by adding CaZrO$_3$ to ceramics, including reduction of the porosity and the sintering temperature, refinement of microstructures and improvement of some electrical properties (Table 1) [4, 20, 21]. As can be seen, sample of CZ10 shows the best property with the maximum Eb (13.37 kV/mm) which is much higher comparing to other BT-based materials. Furthermore, samples with fine-grain microstructures exhibits flat cures for the temperature coefficient of capacitance.

The microscopic EDS analysis is operated from point A to point D, as labeled in Fig. 3. CaZrO$_3$ has a good solubility in BT-based bulk materials. However, for some doping elements that have a low diffusibility, they are inhomogeneously distributed and locate in grain boundaries, for instance, Ca^{2+}, Mn^{2+} and Nb^{5+} have an intense concentration difference between grain interior and grain boundary [4, 22–24]. Concentrated ions at boundaries and surface layer are associated with point defects and lattice distortion, which will yield a strain energy [25]. On account of the stain energy, the formation energy of oxygen vacancies can be lowered to a certain extent and the grain-boundary diffusion coefficient is enhanced. Thus "core–shell" structure is formed, which was observed by Hennings and Rosenstein first in 1984 [26]. But those elements such as Zr^{4+} and Ni^{2+} who have a high diffusibility are almost homogeneously distributed. Those ions
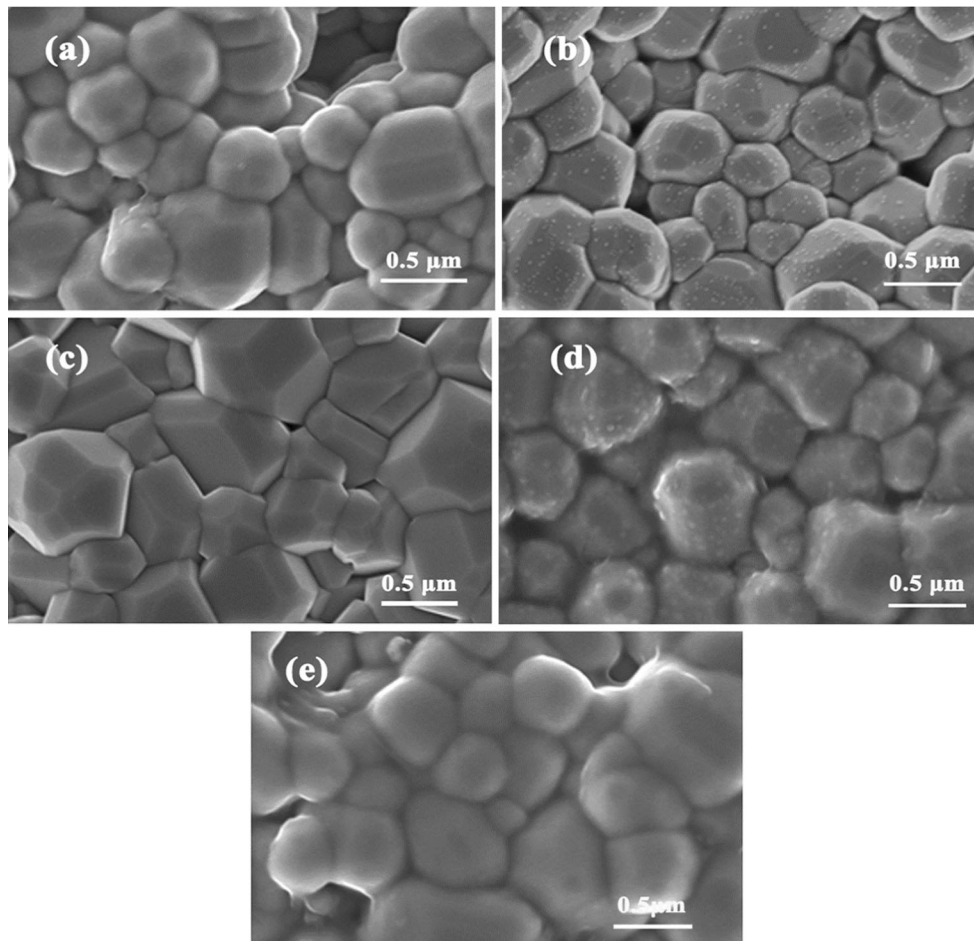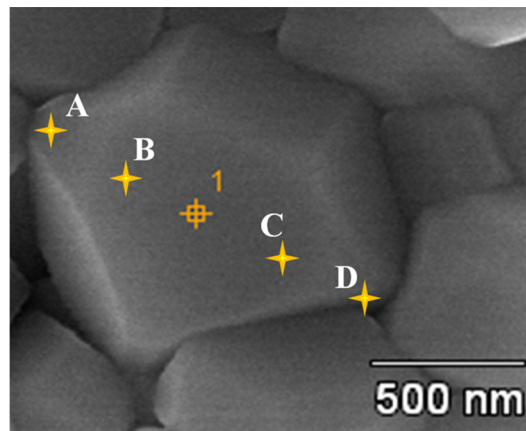
Fig. 2 SEM photos of samples with various amounts of CaZrO₃: **a** 0.0 wt %; **b** 0.5 wt %; **c** 1.0 wt %; **d** 2.0 wt %; **e** 3.0 wt %

Fig. 3 Elements distribution of BaTiO₃-based ceramic sample doped with 1.0 wt % CaZrO₃ (the symbol "—" means element can't be detected at this point)

Element	Atomic percentage				
	A	B	1	C	D
O K	63.85	68.09	67.06	67.58	63.14
Ca K	0.51	0.06	—	0.13	0.51
Ti K	17.81	15.42	16.70	16.40	17.72
Mn K	0.49	—	—	0.05	0.34
Ni K	—	0.55	—	—	—
Zr L	0.67	0.74	0.63	0.58	0.58
Nb L	0.33	0.09	—	0.05	0.17
Ba L	16.33	15.04	15.60	15.22	17.54

mainly concentrate in grain boundaries in form of non-ferroelectric phase, which is proved by E. Brzozowski [27], so that the overall dielectric constant is decreased with the increasing CaZrO₃ content. Further analysis indicates Zr^{4+} plays a major role in aiding sintering, which is mainly attributed to the enhancement of grain-boundary diffusion and the formation of eutectics which is benefit for achieving medium temperature sintering [10, 19].
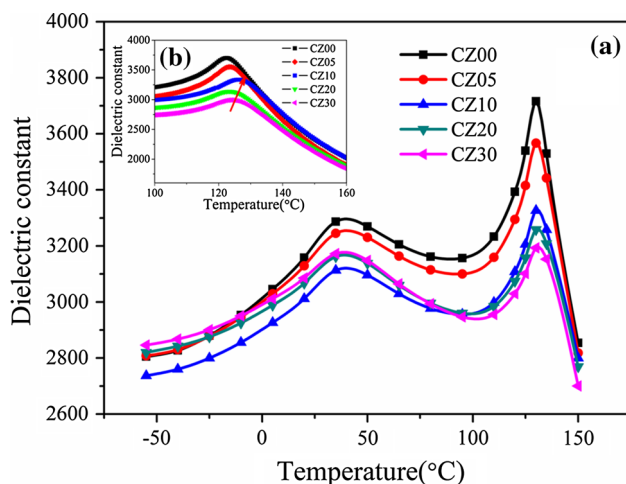
Fig. 4 Temperature dependence of **a** dielectric constant and **b** T_c change for samples with various amounts of CaZrO$_3$ sintered at 1,135 °C

Fig. 5 Temperature dependence of capacitance change for samples with various amounts of CaZrO$_3$ sintered at 1,135 °C

3.3 Dielectric and electrical properties analysis

Main dielectric and electrical properties of samples are listed in Table 1. All samples exhibit low dielectric loss (tanδ no larger than 1.5 %) and the dielectric constant at room temperature reduce with increasing CaZrO$_3$ content. In the case of 1.0 wt % CaZrO$_3$, the maximum $\varepsilon_{20°C}$ achieve to 3,203. Besides, the insulation resistivity (ρ_v) in room temperature increases along with the increase of CaZrO$_3$ content and all rises to 10^{13} Ω cm, especially the sample with 1.0 wt % CaZrO$_3$, which can be attributed to the improvement of ceramic microstructure for BT ceramics with a slightly Ti-excess composition were reported to have a higher sintering density. Furthermore, the doping of CaZrO$_3$ shifts the Curie temperature (T_c) to a higher point. As shown in Fig. 4b, the T_c of the CaZrO$_3$-free sample is about 125 °C. When 1.0 wt % CaZrO$_3$ is doped, the Curie point rise to about 128.5 °C. With the continued increasing CaZrO$_3$ content, the T_c shifts to lower temperature gradually. Noteworthily, the changes of c/a ratio at room temperature of CaZrO$_3$-doped samples show the same discipline in comparison to T_c. The incorporation of CaZrO$_3$ shifts the T_c to a higher point, due to the deformation of crystal structure produced by ion substitution. The reinforcement of tetragonal structure benefits the spontaneous polarization of Ti^{4+} ions, thus shifts the T_c to a higher point. Meanwhile, when the tetragonality is restrained with excess CaZrO$_3$ content, the T_c decreases monotonously.

Figure 4a shows the temperature dependence of the dielectric constant of samples sintered at 1,135 °C for 3 h with the addition of 0–3.0 wt % CaZrO$_3$. The curve shows the same trend, the ε_r-T curves appear two dielectric peaks
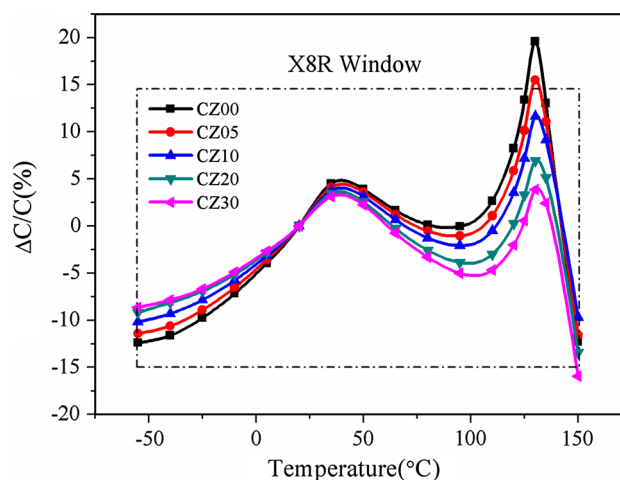
along with the change of temperature, the peak appears in room temperature and the dielectric peak appears in $\sim$130 °C named Curie peak (T_c). Dielectric constant is reduced broadly by increasing the content of CaZrO$_3$, especially dielectric constant at room temperature ($\varepsilon_{20°C}$) indicates a steady decrease with increasing CaZrO$_3$ which is opposite to Yao [6]. We deem that CaZrO$_3$ is a non-ferroelectric dopant and mainly locates at grain shells, the non-ferroelectric phase decreases dielectric constant totally. It can be certificated by the dielectric peak in room temperature that non-ferroelectric phase domain produced when sintering in high temperature.

In addition, with the increase of CaZrO$_3$ content, the dielectric constant peak at T_c is markedly suppressed, and the T_c peak shifts to higher temperature when the CaZrO$_3$ content is less than 1.0 wt %, with continuing doping, T_c peak move left (Fig. 4b). The substitution of Ba^{2+} (1.61 Å, 12 coordinate) with Ca^{2+} (1.34 Å, 12 coordinate) makes the unit cells compact while the substitution of Ti^{4+} (0.605 Å, six coordinate) with Zr^{4+} (0.86 Å, six coordinate) expands the unit cells [6]. As shown in Fig. 3, we deem that CaZrO$_3$ is mainly located in grain shells, and the internal stress induced by the lattice mismatch between cores and shells resulting in the changes of BT lattice parameters in core regions (Table 1). The tensile stress stabilizes the tetragonal phase and shifts T_c to a higher point. Conversely, it can be speculated the compressive stresses shrink the volume of unit cell and shift T_c to a lower point [6, 11].

Figure 5 shows the temperature coefficient of capacitance (TCC) curves for CaZrO$_3$-doped ceramics (0–3.0 wt %) sintered at 1,135 °C for 3 h. As it shows, an increasing of CaZrO$_3$ content yielded a flat TCC curve, with two broad dielectric constant peaks at around 40 and
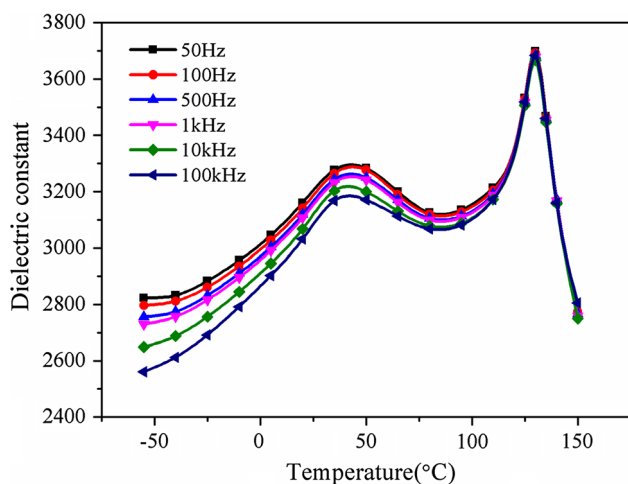
Fig. 6 Frequency dependence of dielectric constant for samples doped by 1.0 wt % CaZrO₃ sintered at 1,135 °C

130 °C, respectively. The CaZrO₃-free sample exhibits a temperature dependence that just not fulfills the X8R specification with temperature variation of capacitance about 20 % at 125 °C. The addition of CaZrO₃ with proper amount can markedly suppress the capacitance variation and smooth the TCC curves thus satisfying the X8R characteristic. As CaZrO₃ concentration increases, the high temperature peak of the variation rate curve of capacitance (about 130 °C) exhibits a continuous compression, and meanwhile, the $\Delta C/C_{20°C}$ at −55 °C decreases while $\Delta C/C_{20°C}$ at 150 °C increases. In the case of 1.0 wt % CaZrO₃, the TCC curve fulfills the X8R window with $\varepsilon_{20°C} = 3{,}203$ and $\tan\delta = 1.019$ %. However, heavy doping with CaZrO₃ may cause a serious suppression of Curie peak which make the TCC curve out of the X8R window at 150 °C.

The variations of relative permittivity of CaZrO₃-doped ceramic samples at various frequencies (50 Hz–100 kHz) are shown in Fig. 6. The permittivity of the sample decreases obviously with the increasing frequency in the low-temperature (−55 to 110 °C), but no significant differences are observed in high-temperature (110–150 °C). The variation of the permittivity of the corresponding frequency in the low-temperature can be qualitatively explained by the Debye's theory. The dielectric-constant peak at the Curie point and the second broad dielectric constant peak at a lower temperature are correlated with the volume fraction of the grain core and shell, respectively, which is proposed by Park et al. [10]. So the experiment results proved the "core–shell" structure in another way: Curves in low-temperature represent non-ferroelectric phase (the shell) produced by ion doping (Ca²⁺, Zr⁴⁺), which affected by frequency significantly. On the contrary, curves in high-temperature mainly affected by pure BT, which is ferroelectric phase (the core), have little difference with frequency [24].

4 Conclusions

Lead-free BT-based ceramics with different amounts of CaZrO₃ (0.0, 0.5, 1.0, 2.0 and 3.0 wt %) were synthesized by conventional solid-state method and well sintered at medium temperature (1,135 °C). The CaZrO₃ have diffused into the BT lattice to form a solid solution, the crystal structure changes gradually from tetragonal to pseudo-cubic with increasing CaZrO₃ content. The c/a ratio shows the same trend, which support to the XRD result. Moreover, the capacitance curves of the samples with a fine grain microstructure had a flattened temperature coefficient. CaZrO₃ content played a crucial role to the stability of high-temperature dielectric properties, which shift the T_c to a higher temperature, and a proper amount of CaZrO₃ additions is needed to suppress the capacitance variation and to make sure the TCC curves satisfies the X8R characteristic. Furthermore, Ca²⁺ and Zr⁴⁺ ions play a major role in aiding sintering. As a result, the 1.0 wt % CaZrO₃-doped samples exhibits the optimal dielectric properties with high dielectric constant $\varepsilon_{20°C} = 3{,}203$, low dielectric loss $\tan\delta = 1.019$ %, and flat temperature-capacitance curve $\Delta C/C \leq \pm 10$ %, −55–150 °C, which satisfy EIA-X8R specification.

References

1. S. Wang, S.R. Zhang, X.H. Zhou, B. Li, Z. Chen, J. Mater. Lett. **60**, 909 (2006)
2. D.H. Choi, A. Baker, M. Lanagan, S. Trolier-Mckinstry, C. Randall, J. Am. Ceram. Soc. **96**, 2197 (2013)
3. W.H. Lee, C.Y. Su, J. Am. Ceram. Soc. **90**, 3345 (2007)
4. L. Zhang, O.P. Thakur, A. Feteira, G.M. Keith, A.G. Mould, Appl. Phys. Lett. **90**, 2914 (2007)
5. C.Y. Chang, H.I. Ho, T.Y. Hsieh, C.Y. Huang, Y.C. Wu, Ceram. Int. **39**, 8245 (2013)
6. G.F. Yao, X.H. Wang, T.Y. Sun, L.T. Li, J. Am. Ceram. Soc. **94**, 3856 (2011)
7. G.F. Yao, X.H. Wang, Y. Yang, L.T. Li, J. Am. Ceram. Soc. **93**, 1697 (2010)
8. S.H. Wu, G.Q. Wang, Y.S. Zhao, J. Mater. Res. **17**, 1550 (2002)
9. S.J. Kuang, X.G. Tang, L.Y. Li, Y.P. Jiang, Q.X. Liu, Scripta Mater. **61**, 68 (2009)
10. K.J. Park, C.H. Kim, Y.J. Yoon, S.M. Song, Y.T. Kim, K.H. Hur, J. Eur. Ceram. Soc. **29**, 1735 (2009)
11. L.B. Ben, D.C. Sinclair, Appl. Phys. Lett. **98**, 092907 (2011)
12. S. Wang, H. Su, L.Y. Chen, H.Y. Yuan, J. Mater. Sci.: Mater. El. **21**, 1159 (2010)
13. B. Tang, S.R. Zhang, Y. Yuan, X.H. Zhou, Y.S. Liang, Sci. China Ser. E **51**, 1451 (2008)
14. Z.Y. Hu, B. Cui, M. Li, L.L. Li, J. Mater. Sci.: Mater. El. **24**, 3850 (2013)
15. C.C. Huang, D.P. Cann, J. Appl. Phys. **104**, 024117 (2008)
16. M. Ganguly, S.K. Rout, T.P. Sinha, S.K. Sharma, H.Y. Park, I.W. Kim, J. Alloy. Compd. **579**, 473 (2013)
17. T.R. Armstrong, R.C. Buchanan, J. Am. Ceram. Soc. **73**, 1268 (1990)

18. C.L. Freeman, J.A. Dawson, H.R. Chen, L.L. Ben, J.H.H. Harding, F.D. Morrison, D.C. Sinclair, A.R. West, Adv. Funct. Mater. **23**, 3925 (2013)
19. J.K. Lee, K.S. Hong, J.W. Jang, J. Am. Ceram. Soc. **84**, 2001 (2001)
20. X.G. Wang, Y. Zhang, X.Z. Song, Z.B. Yuan, T. Ma, Q. Zhang, C.S. Deng, T.X. Liang, J. Eur. Ceram. Soc. **32**, 559 (2012)
21. J.Q. Qi, X.H. Wang, H. Zhang, H. Zou, Z.B. Wang, X.W. Qi, Y. Wang, L.T. Li, H.L.W. Chan, Ceram. Int. **40**, 2747 (2014)
22. Q.H. Zhang, Y.Y. Zhang, F.F. Wang, Y.J. Wang, D. Lin, X.Y. Zhao, H.S. Luo, W.W. Ge, D. Viehland, Appl. Phys. Lett. **95**, 102904 (2009)
23. I.A. Velasco-Davalos, A. Ruediger, J.J. Cruz-Rivera, C. Gomez-Yanez, J. Alloy. Compd. **581**, 56 (2013)
24. M. Cernea, B.S. Vasile, A. Boni, A. Iuga, J. Alloy. Compd. **587**, 553 (2014)
25. M. Bäurer, M. Syha, D. Weygand, Acta Mater. **61**, 5664 (2013)
26. D. Hennings, G. Rosenstein, J. Am. Ceram. Soc. **67**, 249 (1984)
27. E. Brzozowski, M.S. Castro, C.R. Foschini, B. Stojanovic, Ceram. Int. **28**, 773 (2002)